

Beyond Consistency: Inference for the Relative risk functional in Deep Nonparametric Cox Models

Sattwik Ghosal^{*} Xuran Meng[†] and Yi Li[‡]

Abstract

There remain theoretical gaps in deep neural network estimators for the nonparametric Cox proportional hazards model. In particular, it is unclear how gradient-based optimization error propagates to population risk under partial likelihood, how pointwise bias can be controlled to permit valid inference, and how ensemble-based uncertainty quantification behaves under realistic variance decay regimes. We develop an asymptotic distribution theory for deep Cox estimators that addresses these issues. First, we establish nonasymptotic oracle inequalities for general trained networks that link in-sample optimization error to population risk without requiring the exact empirical risk optimizer. We then construct a structured neural parameterization that achieves infinity-norm approximation rates compatible with the oracle bound, yielding control of the pointwise bias. Under these conditions and using the Hájek–Hoeffding projection, we prove pointwise and multivariate asymptotic normality for subsampled ensemble estimators. We derive a range of subsample sizes that balances bias correction with the requirement that the Hájek–Hoeffding projection remain dominant. This range accommodates decay conditions on the single-overlap covariance, which measures how strongly a single shared observation influences the estimator, and is weaker than those imposed in the subsampling literature. An infinitesimal jackknife representation provides analytic covariance estimation and valid Wald-type inference for relative risk contrasts such as log-hazard ratios. Finally, we illustrate the finite-sample implications of the theory through simulations and a real data application.

1 Introduction

High-complexity estimators based on deep neural networks (DNNs) have achieved success across a range of statistical tasks. Although progress has been made in establishing population risk consistency and approximation guarantees in some settings (Schmidt-Hieber, 2020; Farrell et al., 2021), statistical inference remains underdeveloped. In particular, it is not well understood how optimization error arising from gradient-based training is carried into population risk (Allen-Zhu et al., 2019; Arora et al., 2019), how to enforce the pointwise bias control required for valid confidence intervals (Hall, 1992; Cattaneo et al., 2020; Farrell et al., 2021), and how to construct tractable and reliable uncertainty quantification for scientifically relevant targets such as relative-risk contrasts (Lakshminarayanan et al., 2017; Chernozhukov et al., 2018; Wager and Athey, 2018). Moreover, the inferential theory for DNN estimators in the presence of censoring is limited.

We introduce the nonparametric Cox proportional hazards model (Cox, 1972) under independent censoring. Let $\mathbf{X} \in [0, 1]^{p_0}$ denote a vector of (normalized) baseline covariates with dimension

^{*}Department of Biostatistics, University of Michigan; e-mail: ghosal@umich.edu

[†]Department of Biostatistics, University of Michigan; e-mail: xuram@umich.edu

[‡]Department of Biostatistics, University of Michigan; e-mail: yili@umich.edu

p_0 and T_U denote the event time. The nonparametric Cox model (Sleeper and Harrington, 1990; O’Sullivan, 1993; Chen and Zhou, 2007; Chen et al., 2010) specifies the conditional hazard of T_U given \mathbf{X} as

$$\lambda(t | \mathbf{X}) = \lambda_0(t) \exp\{g_0(\mathbf{X})\}, \quad (1.1)$$

where $\lambda_0(\cdot)$ is an unspecified baseline hazard function and $g_0 : [0, 1]^{p_0} \rightarrow \mathbb{R}$ is an unknown function with $g_0(\mathbf{0}) = 0$ for identifiability. We estimate g_0 by \hat{g} over a DNN function class and also consider relative risk comparisons. For two covariate vectors $\mathbf{x}_*^{(1)}$ and $\mathbf{x}_*^{(2)}$, the log-hazard contrast under model (1.1) is

$$\log \frac{\lambda(t | \mathbf{X} = \mathbf{x}_*^{(1)})}{\lambda(t | \mathbf{X} = \mathbf{x}_*^{(2)})} := \psi(\mathbf{x}_*^{(1)}, \mathbf{x}_*^{(2)}) = g_0(\mathbf{x}_*^{(1)}) - g_0(\mathbf{x}_*^{(2)}), \quad (1.2)$$

which provides an interpretable measure of relative risk between the two covariate settings.

Recent semiparametric theory focuses on finite dimensional parameters, treating g_0 as a machine learned nuisance (Chernozhukov et al., 2018). In contrast, inference for g_0 itself, particularly for DNN estimators, remains largely unresolved. Existing methods establish risk consistency but do not control pointwise bias sufficiently to obtain distributional approximations for high-complexity DNN estimators (Zhong et al., 2022; Zhou et al., 2023; Sun et al., 2024; Wu et al., 2024).

We develop inference for DNN estimators with censored survival data (Katzman et al., 2018; Wiegrebe et al., 2024). This setting poses several challenges. First, censoring leads to incomplete observations and complicates the objective function. Second, practical training algorithms yield only approximate empirical risk optimizers, and it remains unclear how the resulting optimization gap carries over to the population risk in Cox models (Schmidt-Hieber, 2020; Kohler and Langer, 2021; Zhong et al., 2022; Meng and Li, 2026). Third, the nonparametric component $g_0(\cdot)$ is estimable at rates slower than $n^{-1/2}$, so classical semiparametric theory (Andersen and Gill, 1982; Bickel et al., 1993; van der Vaart, 1998) does not provide distributional approximations. Valid inference requires linking optimization error to population risk, controlling pointwise bias, and characterizing the covariance of nonlinear functionals. In particular, inference for the contrast $\psi(\mathbf{x}_*^{(1)}, \mathbf{x}_*^{(2)})$ depends on the joint distribution of $\hat{g}(\mathbf{x}_*^{(1)})$ and $\hat{g}(\mathbf{x}_*^{(2)})$. Their dependence, induced by the shared training sample, must be accounted for. We develop a three-part inferential framework to address these challenges.

1. Optimization-to-population risk bridge under partial likelihood. We establish an oracle inequality for DNN estimators trained via gradient-based optimization under the Cox partial likelihood. Existing analyses typically assume access to the exact empirical optimizer (Zhong et al., 2022), which permits a two-step argument: first, uniform convergence establishes consistency, and second, a localized empirical process analysis around the true function yields convergence rates. In contrast, gradient-based training does not guarantee a global optimizer of the empirical objective, preventing a direct application of such localization arguments. Instead, we derive a global bound on the population risk of the form

$$\text{population risk} \lesssim \text{optimization gap} + \text{approximation error} + \text{statistical error},$$

where the optimization gap captures the deviation from exact empirical optimality. The resulting bound is self-referential, in that the population risk appears on both sides of the inequality. We resolve this by combining empirical process techniques for Cox models (Huang, 1999; Zhong et al.,

2022) with Bernstein-type concentration inequalities over suitable coverings of DNN class.

2. **Bias calibration linking population risk and pointwise inference.** We control pointwise bias via sharp L_∞ approximation bounds. By scaling the network architecture (e.g., width and depth), the approximation error is asymptotically dominated by the stochastic fluctuation of the estimator, analogous to undersmoothing in classical nonparametric inference. This renders the approximation term in the oracle inequality negligible for pointwise inference. We further impose a mild alignment condition requiring that the trained network achieve the approximation rate, avoiding underutilization of model capacity during optimization.
3. **Subsample ensemble inference under relaxed single-overlap covariance decay.** We construct a subsampling-based ensemble estimator and analyze its distribution using the Hájek Hoeffding projection. Its variance is characterized by the *single-overlap covariance* introduced in Section 4, which captures dependence between estimators trained on subsamples sharing one observation (Wager and Athey, 2018). Existing ESM theory for generalized nonparametric regression (Meng and Li, 2026) typically assumes near minimal decay of this covariance at rate $1/r$, where r is the subsample size. We relax this requirement and establish asymptotic normality over a broader range of decay rates. A key condition is that r is large enough so that approximation bias is negligible while remaining $o(n)$, so that higher-order U-statistic terms are negligible and the Hájek projection dominates. Under these conditions, we establish multivariate asymptotic normality for finite sets of evaluation points and prove consistency of an infinitesimal jackknife covariance estimator, enabling Wald-type inference for nonlinear contrasts (1.2).

Section 2 reviews DNNs and the nonparametric Cox model. Section 3 introduces the subsample-based ensemble inferential framework. Section 4 presents the theoretical results, including global consistency and asymptotic distributional theory for the ensemble estimator. Sections 5 and 6 illustrate the finite-sample performance through simulations and a real data application. Section 7 concludes. Full proofs and auxiliary lemmas are given in the appendix.

1.1 Notation

Vectors are boldfaced: uppercase bold letters (e.g., \mathbf{X}) represent random vectors, and lowercase bold letters (e.g., \mathbf{x} or \mathbf{x}_*) denote fixed points or realizations. For random \mathbf{X} , $\mathbb{P}_{\mathbf{X}}$ denotes its distribution and $\mathbb{E}_{\mathbf{X}}$ the corresponding expectation. For a vector $\mathbf{x} = (x_1, \dots, x_d)^\top$, define its ℓ_p -, ℓ_∞ -, and ℓ_0 -norms by $|\mathbf{x}|_p = \left(\sum_{j=1}^d |x_j|^p\right)^{1/p}$, $|\mathbf{x}|_\infty = \max_{1 \leq j \leq d} |x_j|$, $|\mathbf{x}|_0 = \sum_{j=1}^d \mathbb{I}(x_j \neq 0)$, where $\mathbb{I}(\cdot)$ is the indicator function; for a function $f : \mathcal{X} \rightarrow \mathbb{R}$, define its L_p norm by $\|f\|_p = \left(\int_{\mathcal{X}} |f(x)|^p dx\right)^{1/p}$, $1 \leq p < \infty$, $\|f\|_\infty = \sup_{x \in \mathcal{X}} |f(x)|$. For a matrix $\mathbf{A} = (a_{ij})$, define $\|\mathbf{A}\|_0 = \sum_{i,j} \mathbb{I}(a_{ij} \neq 0)$, $\|\mathbf{A}\|_\infty = \max_i \sum_j |a_{ij}|$. For two deterministic sequences x_n and a_n , write $x_n = O(a_n)$ if $|x_n/a_n| \leq C$ for a $C > 0$ when n is sufficiently large, and $x_n = o(a_n)$ if $x_n/a_n \rightarrow 0$. For random variables X_n , $X_n = O_p(a_n)$ if for any $\epsilon > 0$ there exists $C > 0$ such that $P(|X_n/a_n| > C) \leq \epsilon$ when n is sufficiently large, and $X_n = o_p(a_n)$ if $X_n/a_n \xrightarrow{p} 0$. For sequences X_n and Y_n , write $X_n \lesssim Y_n$ if $X_n \leq CY_n$ for a $C > 0$ when n is sufficiently large, and $X_n \asymp Y_n$ if $X_n \lesssim Y_n$ and $Y_n \lesssim X_n$. Finally, $a \wedge b = \min\{a, b\}$ and $a \vee b = \max\{a, b\}$.

2 Preliminaries

2.1 Multilayer Neural Networks

Let $L \geq 1$ denote the number of hidden layers and $\mathbf{p} = (p_0, \dots, p_{L+1})$ the corresponding layer widths. With ReLU activation $\sigma(x) = \max\{x, 0\}$ applied componentwise, define the shifted activation $\sigma_{\mathbf{v}}(\mathbf{x}) = \sigma(\mathbf{x} - \mathbf{v})$. We focus on ReLU because of its strong approximation properties and favorable optimization behavior; in particular, its derivative equals one for positive inputs, preventing gradient attenuation during training (Schmidt-Hieber, 2020; Zhong et al., 2022).

A network with architecture (L, \mathbf{p}) is the mapping $f : \mathbb{R}^{p_0} \rightarrow \mathbb{R}^{p_{L+1}}$ defined by

$$f(\mathbf{x}) = \mathcal{W}_L \sigma_{\mathbf{v}_L} \left(\mathcal{W}_{L-1} \sigma_{\mathbf{v}_{L-1}} \left(\dots \mathcal{W}_1 \sigma_{\mathbf{v}_1} (\mathcal{W}_0 \mathbf{x}) \dots \right) \right), \quad (2.1)$$

where $\mathcal{W}_l \in \mathbb{R}^{p_{l+1} \times p_l}$ and $\mathbf{v}_l \in \mathbb{R}^{p_{l+1}}$. Here p_0 denotes the input dimension, p_1, \dots, p_L are the widths of the L hidden layers, and p_{L+1} is the output dimension; for example, in Figure 1, $L = 3$ with $p_0 = 5$, $p_1 = p_2 = 4$, $p_3 = 3$, and $p_4 = 1$.

To mitigate overfitting, we restrict attention to sparsely connected networks. Define the s -sparse network class with envelope F by

$$\mathcal{F}(L, \mathbf{p}, s, F) = \left\{ g \in \mathcal{F}(L, \mathbf{p}) : \sum_{l=0}^L \|\mathcal{W}_l\|_0 + \sum_{l=1}^L \|\mathbf{v}_l\|_0 \leq s, \|g\|_\infty \leq F \right\}, \quad (2.2)$$

where

$$\mathcal{F}(L, \mathbf{p}) = \left\{ g(\mathbf{x}) = f(\mathbf{x}) - f(\mathbf{0}) : f \text{ is a DNN of the form (2.1),} \right. \\ \left. \|\mathcal{W}_l\|_\infty \leq 1 \text{ for } l = 0, \dots, L, \|\mathbf{v}_l\|_\infty \leq 1 \text{ for } l = 1, \dots, L \right\}.$$

By construction, $g(\mathbf{0}) = 0$ for all $g \in \mathcal{F}(L, \mathbf{p})$, which ensures identifiability.

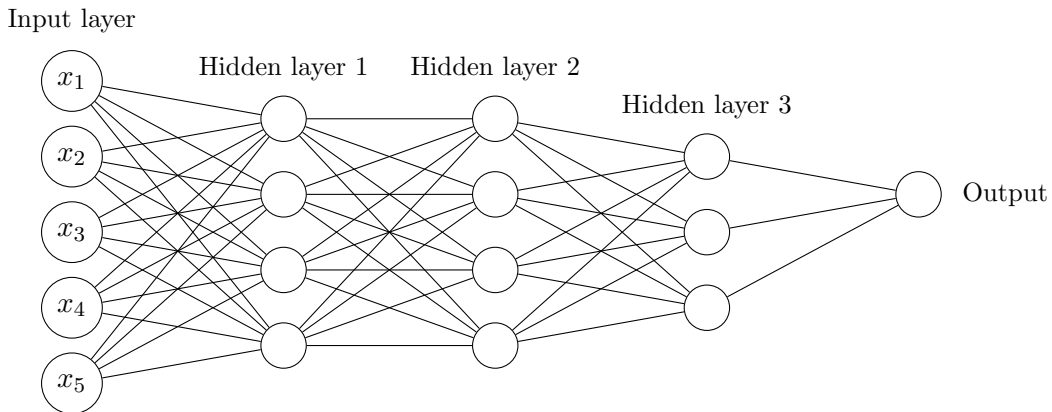


Figure 1: A fully connected neural network with $L = 3$ and $\mathbf{p} = (5, 4, 4, 3, 1)$.

2.2 Nonparametric Cox Models and Hölder Functional Classes

We consider right-censored survival data, where T_U and T_C denote the event time and censoring time, respectively, and $\mathbf{X} \in [0, 1]^{p_0}$ is a p_0 -dimensional covariate vector. We assume that T_U and T_C are conditionally independent given \mathbf{X} (Fleming and Harrington, 2005). We observe n independent and identically distributed (i.i.d.) copies $D_i = (T_i, \Delta_i, \mathbf{X}_i)$ of $D = (T, \Delta, \mathbf{X})$, where $T_i = T_{i,U} \wedge T_{i,C}$ and $\Delta_i = \mathbb{I}(T_{i,U} \leq T_{i,C})$. Let $\mathcal{D}_n = \{D_i\}_{i=1}^n$ denote the sample of size n . We study the nonparametric Cox model (1.1), which extends the classical Cox model (Cox, 1972) by allowing the log-risk function $g_0(\cdot)$ to be an unknown function of \mathbf{X} . To ensure identifiability, we impose $g_0(\mathbf{0}) = 0$. While existing work on nonparametric and DNN-based estimators mainly establishes consistency (Zhong et al., 2022), we develop inference for $g_0(\cdot)$, including uncertainty quantification for pointwise evaluations and contrasts.

We assume that g_0 belongs to a Hölder class $\mathcal{G}_{p_0}^\gamma([0, 1]^{p_0}, K)$ with smoothness $\gamma > 0$ and radius $K > 0$ (Schmidt-Hieber, 2020; Zhong et al., 2022), defined as

$$\mathcal{G}_{p_0}^\gamma([0, 1]^{p_0}, K) = \left\{ g : [0, 1]^{p_0} \rightarrow \mathbb{R} : \sum_{\|\beta\|_1 < \gamma} \|\partial^\beta g\|_\infty + \sum_{\|\beta\|_1 = \lfloor \gamma \rfloor} \sup_{\mathbf{x} \neq \mathbf{y} \in [0, 1]^{p_0}} \frac{|\partial^\beta g(\mathbf{x}) - \partial^\beta g(\mathbf{y})|}{\|\mathbf{x} - \mathbf{y}\|_\infty^{\gamma - \lfloor \gamma \rfloor}} \leq K \right\}.$$

Here $\lfloor \gamma \rfloor$ denotes the integer part of γ , and for a multi-index $\beta = (\beta_1, \dots, \beta_{p_0})^\top \in \mathbb{N}^{p_0}$, $\partial^\beta = \partial^{\beta_1} \dots \partial^{\beta_{p_0}}$.

We further assume that g_0 admits a compositional representation with Hölder-smooth components. For some integer $q \geq 0$ and vectors $\mathbf{d} = (d_0, \dots, d_{q+1}) \in \mathbb{N}_+^{q+2}$, $\mathbf{t} = (t_0, \dots, t_q) \in \mathbb{N}_+^{q+1}$, and $\gamma = (\gamma_0, \dots, \gamma_q) \in \mathbb{R}_+^{q+1}$, we assume

$$g_0 \in \mathcal{G}(q, \mathbf{d}, \mathbf{t}, \gamma, K) = \left\{ g = g^{(q)} \circ \dots \circ g^{(0)} : g^{(i)} = (g_j^{(i)})_j : [a_i, b_i]^{d_i} \rightarrow [a_{i+1}, b_{i+1}]^{d_{i+1}}, \right. \\ \left. g_j^{(i)} \in \mathcal{G}_{t_i}^{\gamma_i}([a_i, b_i]^{t_i}), \quad |a_i|, |b_i| \leq K \right\}. \quad (2.3)$$

The class \mathcal{G} combines Hölder smoothness with a compositional structure, with each $g^{(i)}$ acting on the output of the preceding map, reflecting the layered structure of DNNs (Yarotsky, 2017). The vectors \mathbf{d} and \mathbf{t} specify layer-wise dimensions, and γ encodes smoothness at each level. In a p_0 -variate Cox model (1.1), $g_0 : [0, 1]^{p_0} \rightarrow \mathbb{R}$, so $d_0 = p_0$, $d_{q+1} = 1$, $a_0 = 0$ and $b_0 = 1$. We provide two examples with $q = 2$.

Example 1.

$$g_0(\mathbf{x}) = g_1^{(2)}\left(g_1^{(1)}\left(g_1^{(0)}(x_1, x_2), g_2^{(0)}(x_3, x_4, x_5)\right), g_2^{(1)}\left(g_3^{(0)}(x_6, x_7), g_4^{(0)}(x_8, x_9, x_{10})\right)\right), \quad \mathbf{x} \in [0, 1]^{10}.$$

If all component functions $g_j^{(i)}$ are twice continuously differentiable, then $\gamma = (2, 2, 2)$, $\mathbf{d} = (10, 4, 2, 1)^\top$, and $\mathbf{t} = (3, 2, 2)^\top$.

Example 2.

$$g_0(\mathbf{x}) = g_1^{(2)}\left(g_1^{(1)}\left(g_1^{(0)}(x_1, x_2), g_2^{(0)}(x_3)\right), g_2^{(1)}\left(g_3^{(0)}(x_4, x_5), g_4^{(0)}(x_6)\right)\right), \quad \mathbf{x} \in [0, 1]^6,$$

where we suppose each $g_j^{(i)}$ has Hölder smoothness $\gamma_i = \frac{3}{2}$. Hence, $\boldsymbol{\gamma} = (\frac{3}{2}, \frac{3}{2}, \frac{3}{2})$, $\mathbf{d} = (6, 4, 2, 1)^\top$, and $\mathbf{t} = (2, 2, 2)^\top$.

The composite-smoothness class $\mathcal{G}(q, \mathbf{d}, \mathbf{t}, \boldsymbol{\gamma}, K)$ subsumes standard nonparametric models, including additive structures (Stone, 1985) and nested compositional regressions (Horowitz and Mammen, 2007). Related work extends this framework to broader hierarchical compositions beyond the classical Hölder setting (Kohler and Langer, 2021).

Define the effective smoothness at level i by

$$\gamma_i^* = \gamma_i \prod_{l=i+1}^q (\gamma_l \wedge 1),$$

which represents the Hölder smoothness associated with level i after attenuation through subsequent compositions. With a training sample of size n , define

$$\phi_n = \max_{i=0, \dots, q} n^{-2\gamma_i^*/(2\gamma_i^* + t_i)}, \quad (2.4)$$

which is the minimax-optimal estimation rate, up to logarithmic factors, for deep ReLU estimators (Schmidt-Hieber, 2020). Writing $\phi_n = n^{-c_{\text{eff}}}$ gives

$$c_{\text{eff}} = \min_{i=0, \dots, q} \frac{2\gamma_i^*}{2\gamma_i^* + t_i}, \quad i_{\text{eff}} = \arg \min_{0 \leq i \leq q} \frac{2\gamma_i^*}{2\gamma_i^* + t_i}. \quad (2.5)$$

Here, i_{eff} identifies the bottleneck level in the compositional structure, and c_{eff} determines the overall rate $\phi_n = n^{-c_{\text{eff}}}$. Thus, the slowest level in the Hölder hierarchy governs this overall rate. It also sets the scale of the optimal approximation bias as stated in Theorem 1.

3 Inference on DNN Estimates via an Ensemble Subsampling Learner

We estimate $g_0(\cdot)$ in model (1.1) by maximizing the Cox partial likelihood over the DNN function class $\mathcal{F}(L, s, \mathbf{p}, F)$ defined in (2.2). For $g : [0, 1]^{p_0} \rightarrow \mathbb{R}$, the log partial likelihood is

$$L_n(g) = n^{-1} \sum_{i=1}^n \Delta_i \left[g(\mathbf{X}_i) - \log \left\{ \sum_{j: T_j \geq T_i} \exp\{g(\mathbf{X}_j)\} \right\} \right]. \quad (3.1)$$

The empirical optimizer is

$$\hat{g}_{\text{opt}} = \arg \max_{g \in \mathcal{F}(L, \mathbf{p}, s, F)} L_n(g). \quad (3.2)$$

In practice, DNNs are trained by stochastic gradient methods and may not attain \hat{g}_{opt} . To quantify the resulting optimization error, we define the expected optimization gap

$$\mathcal{Q}_n(\hat{g}, \hat{g}_{\text{opt}}) := \mathbb{E}_{\mathcal{D}_n} \{L_n(\hat{g}_{\text{opt}}) - L_n(\hat{g})\},$$

so that $\mathcal{Q}_n(\hat{g}, \hat{g}_{\text{opt}}) \geq 0$, with equality if $\hat{g} = \hat{g}_{\text{opt}}$. When the context is clear, we write $\mathcal{Q}_n(\hat{g}) := \mathcal{Q}_n(\hat{g}, \hat{g}_{\text{opt}})$.

Unlike separable losses, (3.1) does not decompose into a sum of independent contributions due to risk-set coupling, and standard empirical process arguments do not apply. To isolate this dependence, we rewrite the partial likelihood as

$$L_n(g) = n^{-1} \sum_{i=1}^n \Delta_i \ell_n(T_i, \mathbf{X}_i; g) - n^{-1} \sum_{i=1}^n \Delta_i, \quad (3.3)$$

where

$$\ell_n(t, \mathbf{X}; g) = g(\mathbf{X}) - \log S_n^{(0)}(t; g), \quad S_n^{(0)}(t; g) = n^{-1} \sum_{j=1}^n Y_j(t) \exp\{g(\mathbf{X}_j)\},$$

and $Y_j(t) = \mathbb{I}(T_j \geq t)$. Since the second term in (3.3) does not depend on g , we work with

$$L_n(g) = n^{-1} \sum_{i=1}^n \Delta_i \ell_n(T_i, \mathbf{X}_i; g),$$

which yields the same optimizer as (3.2).

We define the population counterpart of $L_n(\cdot)$ as

$$L_0(g) = \mathbb{E}_D\{\Delta \ell_0(T, \mathbf{X}; g)\}, \quad \ell_0(t, \mathbf{X}; g) = g(\mathbf{X}) - \log S^{(0)}(t; g),$$

for $0 \leq t \leq \tau$, where τ is the study end time (Condition 1), and

$$S^{(0)}(t; g) = \mathbb{E}_D\{Y(t) \exp\{g(\mathbf{X})\}\}, \quad Y(t) = \mathbb{I}(T \geq t).$$

The population risk of any fixed function g is

$$R(g, g_0) = L_0(g_0) - L_0(g),$$

which is nonnegative (Lemma 1 in appendix). For a data-dependent estimator \hat{g} , the risk $R(\hat{g}, g_0)$ is random, and we consider its expectation

$$\mathbb{E}_{\mathcal{D}_n}[R(\hat{g}, g_0)],$$

which we refer to as the population risk of \hat{g} .

Uniform convergence of $S_n^{(0)}(t; g)$ to $S^{(0)}(t; g)$ over $t \in [0, \tau]$ allows the data-dependent risk-set average to be replaced by its deterministic limit, so that $L_n(g)$ can be treated as an empirical process with a remainder term, whose magnitude we quantify for DNN estimators.

Inference based on \hat{g} is challenging because it lacks a tractable influence-function representation and its sampling variability is difficult to characterize. By averaging DNN estimators trained on subsamples, ESM stabilizes the estimator and yields an approximate linear representation via its first-order Hájek projection, enabling statistical inference.

3.1 Estimation and Inference via Ensemble Subsampling

For a fixed covariate point $\mathbf{x}_* \in [0, 1]^{p_0}$ and a pair $\mathbf{x}_*^{(1)}, \mathbf{x}_*^{(2)} \in [0, 1]^{p_0}$, we introduce an ensemble subsampling method (ESM; Algorithm 1) to estimate $g_0(\mathbf{x}_*)$ and conduct inference for both $g_0(\mathbf{x}_*)$ and the log-hazard ratio $\psi(\mathbf{x}_*^{(1)}, \mathbf{x}_*^{(2)}) = g_0(\mathbf{x}_*^{(1)}) - g_0(\mathbf{x}_*^{(2)})$. The ensemble estimator \hat{g}_B aggregates

subsample estimators $\{\hat{g}^b\}$ trained on overlapping subsets of \mathcal{D}_n , and thus forms a sum of dependent terms. However, \hat{g}_B has the structure of an incomplete U-statistic over subsamples. This enables a Hájek projection (Wager and Athey, 2018), which decomposes \hat{g}_B into a first-order term, a sum of independent influence contributions, and an asymptotically negligible higher-order remainder. The linear representation characterizes the asymptotic distribution.

Algorithm 1: Ensemble Subsampling

1: **Input:** Observed data $\mathcal{D}_n = \{(T_i, \Delta_i, \mathbf{X}_i) : i = 1, \dots, n\}$, subsample size r , number of subsamples B .

2: **Subsampling:** Let $\mathcal{I} = \{1, \dots, n\}$ index observations. Using subset sampling, randomly generate B subsets $\mathcal{I}^b \subset \mathcal{I}$ with $b = 1, \dots, B$.

3: **Model Training:**

For each $1 \leq b \leq B$, we maximize the subsample partial likelihood $L_r(g; \mathcal{I}^b)$ defined from (3.1) on the observations indexed by \mathcal{I}^b . The optimization is performed over $\mathcal{F}(L, \mathbf{p}, s, F)$ using a gradient-based algorithm such as SGD. Let \hat{g}^b denote the resulting (approximate) solution,

$$\hat{g}^b \approx \hat{g}_{\text{opt}}^b := \arg \max_{g \in \mathcal{F}(L, \mathbf{p}, s, F)} L_r(g; \mathcal{I}^b), \quad (3.4)$$

so that

$$\mathcal{Q}_r(\hat{g}^b, \hat{g}_{\text{opt}}^b) \leq \mathcal{Q}_r^{\text{opt}}, \quad (3.5)$$

where $\mathcal{Q}_r^{\text{opt}}$ quantifies the optimization error.

4: **Ensemble Estimator:** Aggregate the subsample estimators to form the ensemble estimate for any fixed $\mathbf{x}_* \in [0, 1]^{p_0}$

$$\hat{g}_B(\mathbf{x}_*) = \frac{1}{B} \sum_{b=1}^B \hat{g}^b(\mathbf{x}_*). \quad (3.6)$$

The corresponding log-hazard ratio (contrast) estimator for two profiles $\mathbf{x}_*^{(1)}$ and $\mathbf{x}_*^{(2)}$ is

$$\hat{\psi}_B(\mathbf{x}_*^{(1)}, \mathbf{x}_*^{(2)}) = \hat{g}_B(\mathbf{x}_*^{(1)}) - \hat{g}_B(\mathbf{x}_*^{(2)}). \quad (3.7)$$

5: **Variance Estimation:** Estimate the asymptotic pointwise variance $\hat{\sigma}^2(\mathbf{x}_*)$ and the contrast variance $\hat{\sigma}_{1,2}^2$ using the infinitesimal jackknife (IJ), which leverages the ESM subsampling structure to provide uncertainty quantification.

6: **Confidence Interval (CI) Construction:** Compute the approximate $(1 - \alpha) \times 100\%$ CIs:

$$\begin{aligned} \text{CI}(g_0(\mathbf{x}_*)) &= \left[\hat{g}_B(\mathbf{x}_*) - c_\alpha \hat{\sigma}(\mathbf{x}_*), \hat{g}_B(\mathbf{x}_*) + c_\alpha \hat{\sigma}(\mathbf{x}_*) \right], \\ \text{CI}(\psi(\mathbf{x}_*^{(1)}, \mathbf{x}_*^{(2)})) &= \left[\hat{\psi}_B(\mathbf{x}_*^{(1)}, \mathbf{x}_*^{(2)}) - c_\alpha \hat{\sigma}_{1,2}, \hat{\psi}_B(\mathbf{x}_*^{(1)}, \mathbf{x}_*^{(2)}) + c_\alpha \hat{\sigma}_{1,2} \right], \end{aligned}$$

where $0 < \alpha < 1$ and c_α denotes the $(1 - \alpha/2)$ quantile of standard normal. With $\frac{\lambda(t|\mathbf{x}_*^{(1)})}{\lambda(t|\mathbf{x}_*^{(2)})} = \exp(\psi(\mathbf{x}_*^{(1)}, \mathbf{x}_*^{(2)}))$, the corresponding CI for relative risk is $[\exp(L), \exp(U)]$, where L and U are the lower and upper bounds of $\text{CI}(\psi(\mathbf{x}_*^{(1)}, \mathbf{x}_*^{(2)}))$, respectively.

Enumerating all $B^* = \binom{n}{r}$ subsets is infeasible, so we draw B random subsets $\mathcal{I}^{b_1}, \dots, \mathcal{I}^{b_B} \subset \mathcal{I} = \{1, \dots, n\}$ with $|\mathcal{I}^b| = r$. The ESM estimator is defined as the average of the corresponding

subsample estimators in (3.6).

We estimate the asymptotic variance of the ensemble estimate $\widehat{g}_B(\mathbf{x}_*)$ using the bias-corrected infinitesimal jackknife (IJ) variance estimator, denoted as $\widehat{\sigma}^2(\mathbf{x}_*)$. Define

$$Z_{ji}(\mathbf{x}_*) = (J_{ji} - J_{\cdot i})(\widehat{g}^{bj}(\mathbf{x}_*) - \widehat{g}_B(\mathbf{x}_*)), \quad \widehat{V}_i(\mathbf{x}_*) = \frac{1}{B} \sum_{j=1}^B Z_{ji}(\mathbf{x}_*),$$

where $J_{ji} = I(i \in \mathcal{I}^{bj})$ is the subsample inclusion indicator for replicate j , and $J_{\cdot i} = B^{-1} \sum_{j=1}^B J_{ji}$. The pointwise IJ variance is then given by

$$\widehat{\sigma}^2(\mathbf{x}_*) = \frac{n(n-1)}{(n-r)^2} \left\{ \sum_{i=1}^n \widehat{V}_i^2(\mathbf{x}_*) - \frac{1}{B(B-1)} \sum_{i=1}^n \sum_{j=1}^B (Z_{ji}(\mathbf{x}_*) - \widehat{V}_i(\mathbf{x}_*))^2 \right\}. \quad (3.8)$$

Consequently, to evaluate the relative risk between two covariate profiles, we estimate the variance of the contrast $\widehat{\psi}_B(\mathbf{x}_*^{(1)}, \mathbf{x}_*^{(2)}) = \widehat{g}_B(\mathbf{x}_*^{(1)}) - \widehat{g}_B(\mathbf{x}_*^{(2)})$ as

$$\widehat{\sigma}_{1,2}^2 = \widehat{\sigma}^2(\mathbf{x}_*^{(1)}) + \widehat{\sigma}^2(\mathbf{x}_*^{(2)}) - 2\widehat{\tau}(\mathbf{x}_*^{(1)}, \mathbf{x}_*^{(2)}), \quad (3.9)$$

where

$$\begin{aligned} \widehat{\tau}(\mathbf{x}_*^{(1)}, \mathbf{x}_*^{(2)}) &= \frac{n(n-1)}{(n-r)^2} \left\{ \sum_{i=1}^n \widehat{V}_i(\mathbf{x}_*^{(1)}) \widehat{V}_i(\mathbf{x}_*^{(2)}) \right. \\ &\quad \left. - \frac{1}{B(B-1)} \sum_{i=1}^n \sum_{j=1}^B (Z_{ji}(\mathbf{x}_*^{(1)}) - \widehat{V}_i(\mathbf{x}_*^{(1)}))(Z_{ji}(\mathbf{x}_*^{(2)}) - \widehat{V}_i(\mathbf{x}_*^{(2)})) \right\}. \end{aligned} \quad (3.10)$$

The variance framework in (3.8)-(3.10) extends Meng and Li (2026) to account for joint dependence across multiple evaluations. The scaling factors correct Monte Carlo and finite-sample bias, enabling valid inference when $B \gtrsim n$. Consistency of this covariance estimator is established later.

4 Theoretical Results

We establish asymptotic results for the ESM estimators (3.6) and (3.7). To characterize their dependence structure, we introduce covariance measures that quantify the influence of individual observations.

Let $D_i = (T_i, \Delta_i, \mathbf{X}_i)$, $i = 1, \dots, n$, be i.i.d. observations. Define the single-overlap covariance measures

$$\begin{aligned} \zeta_r^{(1)}(\mathbf{x}_*) &= \text{Cov}\{\widehat{g}(\mathbf{x}_*; D_1, \dots, D_r), \widehat{g}(\mathbf{x}_*; D_1, D'_2, \dots, D'_r)\}, \\ \zeta_r^{(1)}(\mathbf{x}_*, \mathbf{x}'_*) &= \text{Cov}\{\widehat{g}(\mathbf{x}_*; D_1, \dots, D_r), \widehat{g}(\mathbf{x}'_*; D_1, D'_2, \dots, D'_r)\}, \end{aligned} \quad (4.1)$$

where $\mathbf{x}_*, \mathbf{x}'_* \in [0, 1]^{p_0}$ are fixed evaluation points, and D'_i are independent copies of D_i . Here $\widehat{g}(\mathbf{x}_*; D_1, \dots, D_r)$ denotes the estimator trained on $\{D_1, \dots, D_r\}$ and evaluated at \mathbf{x}_* .

These quantities measure the covariance between estimators trained on subsamples that share one observation and differ in all remaining entries. They capture the leading-order dependence induced by overlap in the subsampling procedure and are central to the Hájek expansion of the resulting U-statistic (Wager and Athey, 2018).

Condition 1. Assume the study ends at time τ such that there exists $\varepsilon_0 > 0$ satisfying

$$P(\Delta = 1 \mid \mathbf{X}) \geq \varepsilon_0 \quad \text{and} \quad P(T_U \geq \tau \mid \mathbf{X}) \geq \varepsilon_0,$$

almost surely with respect to $\mathbb{P}_{\mathbf{X}}$; we also impose the condition $g_0(\mathbf{0}) = 0$.

Condition 1 imposes a standard nondegeneracy condition (Andersen and Gill, 1982), ensuring that the probabilities of failure and of remaining at risk up to time τ are uniformly bounded away from zero, thereby preventing degeneration of the risk-set and partial-likelihood processes. The constraint $g_0(\mathbf{0}) = 0$ ensures identifiability of model (1.1).

To characterize the approximation capacity of the network, we impose architectural constraints on the DNN class in the following Condition 2. In particular, we introduce a hyper parameter $\delta \geq 0$. The case $\delta = 0$ corresponds to the baseline regime achieving the minimax-optimal rate (Schmidt-Hieber, 2020; Zhong et al., 2022), whereas $\delta > 0$ yields an overparameterized architecture required for subsequent analysis.

Condition 2. With g_0 specified in (2.3), the network class $\mathcal{F}(L, \mathbf{p}, s, F)$ is required to satisfy the following structural conditions for some $\delta \geq 0$,

- $\log_2 n \lesssim L \lesssim \log^\mu(n)$, for some $\mu > 1$,
- $n^{1+\delta} \phi_n \lesssim \min_{1 \leq i \leq L} p_i \leq \max_{1 \leq i \leq L} p_i \lesssim n$,
- $s \asymp n^{1+\delta} \phi_n \log n$,
- $F \geq \max\{K, 1\}$.

We define the *optimal network* in $\mathcal{F}(L, \mathbf{p}, s, F)$ that best approximates g_0 :

$$g_{\text{apx}} \in \arg \min_{g \in \mathcal{F}(L, \mathbf{p}, s, F)} \|g - g_0\|_\infty$$

and use the optimal approximation error, $\|g_{\text{apx}} - g_0\|_\infty$, to measure the approximation capability of $\mathcal{F}(L, \mathbf{p}, s, F)$. We establish a bound for $\|g_{\text{apx}} - g_0\|_\infty$ and show that increasing δ sharpens this bound.

Theorem 1 (Bound of Optimal Approximation Error). *Let the true function g_0 be specified in (2.3) with $g_0(\mathbf{0}) = 0$. Under Condition 2, it holds that*

$$\|g_{\text{apx}} - g_0\|_\infty^2 \lesssim \phi_n^{1+\eta},$$

where $\eta = \frac{2\delta \gamma_{i_{\text{eff}}}^*}{t_{i_{\text{eff}}} c_{\text{eff}}}$, with c_{eff} and i_{eff} defined in (2.5).

Theorem 1 characterizes the approximation capability of $\mathcal{F}(L, \mathbf{p}, s, F)$. At the minimax sparsity level ($\delta = 0$), we have $\eta = 0$ so that $\|g_{\text{apx}} - g_0\|_\infty = O(\phi_n^{1/2})$. For $\delta > 0$, overparameterization sharpens this bound to $O(\phi_n^{(1+\eta)/2})$. We next establish a non-asymptotic population risk bound for any estimator $\hat{g} \in \mathcal{F}(L, \mathbf{p}, s, F)$.

Theorem 2. *Under Conditions 1 and 2 for $0 \leq \delta < c_{\text{eff}}$, for any estimator $\hat{g} \in \mathcal{F}(L, \mathbf{p}, s, F)$, there exist constants $c^*, C_1^*, C_2^* > 0$, depending only on the network bound F and the structural constants*

defined in Condition 2, such that the population risk satisfies

$$\max \left\{ 0, \underbrace{\frac{1}{2} \mathcal{Q}_n(\hat{g}, \hat{g}_{opt})}_{\text{optimization gap}} - \underbrace{c^* \phi_n n^\delta L \log^2(n)}_{\text{statistical error}} \right\} \\ \leq \mathbb{E}_{\mathcal{D}_n} [R(\hat{g}, g_0)] \leq \underbrace{2 \mathcal{Q}_n(\hat{g}, \hat{g}_{opt})}_{\text{optimization gap}} + \underbrace{C_1^* \|g_{apx} - g_0\|_\infty^2}_{\text{approximation error}} + \underbrace{C_2^* \phi_n n^\delta L \log^2(n)}_{\text{statistical error}}. \quad (4.2)$$

Theorem 2 establishes that the population risk is bounded by the optimization gap together with approximation and statistical error terms, and clarifies the role of δ . When $\delta = 0$ and the expected optimization error \mathcal{Q}_n is small, the bound attains the minimax rate $O(\phi_n L \log^2 n)$ (Zhong et al., 2022). For $0 < \delta < c_{\text{eff}}$, the rate increases to $O(\phi_n n^\delta L \log^2 n)$ but still vanishes since $\phi_n n^\delta L \log^2 n = o(1)$. While the oracle inequality provides global control of the population risk, its local Kullback–Leibler structure induces quadratic curvature (Lemma 3 in appendix), yielding pointwise error bounds in the following corollary and enabling valid inference after bias calibration.

Corollary 1 (Pointwise Mean Squared Error Bound). *Suppose the conditions of Theorem 2 hold with $0 \leq \delta < c_{\text{eff}}$, and let $\hat{g} \in \mathcal{F}(L, \mathbf{p}, s, F)$ satisfy $\mathcal{Q}_n(\hat{g}, \hat{g}_{opt}) \leq C_1^* \phi_n n^\delta L \log^2 n$ for some constant $C_1^* > 0$. For any slowly diverging sequence $M_n \rightarrow \infty$, if $\mathbf{x}_* \sim \mathbb{P}_{\mathbf{X}}$ and is independent of \mathcal{D}_n , then the pointwise mean squared error satisfies*

$$\mathbb{E}_{\mathcal{D}_n} \left[(\hat{g}(\mathbf{x}_*) - g_0(\mathbf{x}_*))^2 \right] \leq M_n \phi_n n^\delta L \log^2 n$$

with probability at least $1 - M_n^{-1}$ with respect to $\mathbb{P}_{\mathbf{X}}$.

Let

$$\mathcal{B}_{n,\delta} = \left\{ \mathbf{x}_* \in [0, 1]^{p_0} : \mathbb{E}_{\mathcal{D}_n} \left[(\hat{g}(\mathbf{x}_*) - g_0(\mathbf{x}_*))^2 \right] \leq M_n \phi_n n^\delta L \log^2 n \right\} \quad (4.3)$$

denote the subset characterized by Corollary 1, which satisfies $\mathbb{P}_{\mathbf{X}}(\mathcal{B}_{n,\delta}) \geq 1 - M_n^{-1}$. For $\mathbf{x}_* \in \mathcal{B}_{n,\delta}$, the pointwise MSE vanishes when $0 \leq \delta < c_{\text{eff}}$. To establish asymptotic normality at \mathbf{x}_* , however, the pointwise bias must also decay at a suitable rate. Because the estimator \hat{g}^b in (3.6) aggregates base learners trained on subsamples via gradient-based optimization, both the statistical estimation bias and the algorithmic optimization bias need to be controlled at the subsample level.

Condition 3. *For each subsample \mathcal{D}_r (indexed by \mathcal{I}^b) with size r , we assume the pointwise estimation bias of the trained estimator $\hat{g}^b \in \mathcal{F}(L, \mathbf{p}, s, F)$ defined in (3.4) is governed by the optimal network g_{apx} . For any target point $\mathbf{x}_* \in [0, 1]^{p_0}$,*

$$\left| \mathbb{E}_{\mathcal{D}_r} [\hat{g}^b(\mathbf{x}_*)] - g_{apx}(\mathbf{x}_*) \right| \lesssim \{A_r(g_{apx}, \mathbf{x}_*)\}^{1-\xi_r},$$

for a small $0 < \xi_r < 1$, where $A_r(g_{apx}, \mathbf{x}_*) = |g_{apx}(\mathbf{x}_*) - g_0(\mathbf{x}_*)|$ is the pointwise approximation error of g_{apx} at the subsample level r .

Condition 4. *For each subsample \mathcal{D}_r (indexed by \mathcal{I}^b) with size r , the maximum optimization error $\mathcal{Q}_r^{\text{opt}}$ defined in (3.5) satisfies*

$$\mathcal{Q}_r^{\text{opt}} \lesssim \phi_r r^\delta L \log^2 r.$$

Condition 3 is anchored at the approximation benchmark g_{apx} , the best achievable element in $\mathcal{F}(L, \mathbf{p}, s, F)$. It requires that, on average, the trained estimator is close to g_{apx} , thereby separating approximation error from training error. This formulation is intrinsic to the function class and does not impose an artificial centering at g_0 . Any additional deviation reflects optimization deficiency rather than the approximation limit and cannot be absorbed into the bias term, so the condition is necessary to control bias at the scale required for asymptotic normality. As in classical nonparametric inference (Wasserman, 2006), asymptotic normality requires undersmoothing so that the squared bias is negligible relative to the variance. Under the minimax regime ($\delta = 0$), $\|g_{\text{apx}} - g_0\|_\infty = O(\phi_r^{1/2})$, yielding pointwise bias $O(\phi_r^{(1-\xi_r)/2})$, which is not negligible relative to the variance. Thus, an undersmoothed regime ($\delta > 0$) is required, reflecting the same bias–variance tradeoff as in classical settings. Condition 4 controls the optimization gap by requiring that the trained estimator attains the statistical scale of the oracle bound. This condition is stated in terms of the empirical objective actually optimized in practice and does not assume exact minimization. Without such control, the optimization error would enter the leading term of the risk and prevent valid bias calibration, making it necessary for inference.

Condition 5. Assume that $B \gtrsim n$, $r = n^\alpha$ for $0 < \alpha < 1$, and the single-overlap covariance satisfies $\inf_{\mathbf{x}_* \in [0,1]^{p_0}} \zeta_r^{(1)}(\mathbf{x}_*) \gtrsim r^{-\nu}$ for some $\nu \geq 1$.

Condition 5 imposes standard U-statistic scaling so that the first-order Hájek projection dominates the asymptotic expansion, and Monte Carlo variability from ensembling is asymptotically negligible. Because the DNN class admits a bounded envelope, the Hájek decomposition implies that the leading covariance is $O(1/r)$, yielding the natural lower bound $\nu \geq 1$.

Theorem 3. Suppose g_0 belongs to the class (2.3) with $g_0(\mathbf{0}) = 0$. Let \hat{g}_B be the ensemble estimator defined in (3.6) based on B subsamples of size r , and let $\mathcal{B}_{r,\delta}$ be defined in (4.3) with subsample size r . Assume Condition 2 holds with hyper parameter $\delta \in (\frac{c_{\text{eff}}(1-c_{\text{eff}})}{2-c_{\text{eff}}}, c_{\text{eff}})$, and Conditions 3–5 hold at subsample size r . Let $m_0 = c_{\text{eff}}(1+\eta)(1-\xi_r)$. Then, with $\nu \in (1, 1 + \frac{m_0}{2})$, for any $\alpha \in (\alpha_{\text{lower}}, \alpha_{\text{upper}})$ and any fixed $\mathbf{x}_* \in \mathcal{B}_{r,\delta}$, it holds that

$$\sqrt{\frac{n}{r^2 \zeta_r^{(1)}(\mathbf{x}_*)}} (\hat{g}_B(\mathbf{x}_*) - g_0(\mathbf{x}_*)) \xrightarrow{d} \mathcal{N}(0, 1),$$

where

$$\alpha_{\text{lower}} = \frac{1}{2 - \nu + m_0}, \quad \alpha_{\text{upper}} = \frac{1}{\nu + c_{\text{eff}} - \delta}.$$

This range reflects two competing requirements in ESM. The lower bound $\alpha > \alpha_{\text{lower}}$ arises from bias control: the subsample size must be sufficiently large so that the bias is asymptotically negligible. In contrast, the upper bound $\alpha < \alpha_{\text{upper}}$ is imposed by the need for Hájek domination, requiring the variance of the remainder to vanish. A similar tradeoff appears in random forests, where the single-overlap covariance decays at rate $1/\{r(\log r)^{p_0}\}$ (i.e., $\nu \approx 1$) (Wager and Athey, 2018). In our setting, a nonempty admissible interval $(\alpha_{\text{lower}}, \alpha_{\text{upper}})$ is ensured when $\nu < 1 + \frac{m_0}{2}$, which guarantees separation between the bias and variance constraints. The parameter δ governs this tradeoff through its effect on approximation: when δ is small, the approximation bias decays more slowly, increasing α_{lower} and requiring larger subsamples; as δ increases, bias decays faster due to undersmoothing, but this enlarges the projection remainder variance, which decreases α_{upper} . Consequently, more aggressive undersmoothing narrows the admissible range for α .

At fixed evaluation points $\mathbf{x}_*^{(1)}, \dots, \mathbf{x}_*^{(p)} \in [0, 1]^{p_0}$, define the vectors of ensemble estimators and true function values as

$$\widehat{\mathbf{g}}_B := \begin{pmatrix} \widehat{g}_B(\mathbf{x}_*^{(1)}) \\ \vdots \\ \widehat{g}_B(\mathbf{x}_*^{(p)}) \end{pmatrix}, \quad \mathbf{g}_0 := \begin{pmatrix} g_0(\mathbf{x}_*^{(1)}) \\ \vdots \\ g_0(\mathbf{x}_*^{(p)}) \end{pmatrix}. \quad (4.4)$$

Condition 6. Let Ψ_r denote the $p \times p$ single-overlap covariance matrix evaluated at $\mathbf{x}_*^{(1)}, \dots, \mathbf{x}_*^{(p)}$, with entries $(\Psi_r)_{ij} = \zeta_r^{(1)}(\mathbf{x}_*^{(i)}, \mathbf{x}_*^{(j)})$ for $1 \leq i, j \leq p$. With $\zeta_r^{(1)}(\mathbf{x}_*) = \zeta_r^{(1)}(\mathbf{x}_*, \mathbf{x}_*)$, define $\mathbf{D}_r = \text{diag}\{\zeta_r^{(1)}(\mathbf{x}_*^{(1)}), \dots, \zeta_r^{(1)}(\mathbf{x}_*^{(p)})\}$. Let $\mathbf{R}_r = \mathbf{D}_r^{-1/2} \Psi_r \mathbf{D}_r^{-1/2}$ denote the normalized single-overlap covariance matrix. We assume \mathbf{R}_r is uniformly well-conditioned, i.e., $\lambda_{\min}(\mathbf{R}_r) \geq c_0 > 0$ for all sufficiently large r , where $\lambda_{\min}(\mathbf{R}_r)$ denotes the minimum eigenvalue of \mathbf{R}_r .

Condition 6 is a standard nondegeneracy condition ensuring that the estimates at the p evaluation points are not perfectly correlated, thereby yielding a well-defined limiting multivariate normal distribution (Jacot et al., 2018). We extend Theorem 3 to the multivariate setting by establishing asymptotic normality of $\widehat{\mathbf{g}}_B$ in (4.4).

Theorem 4. Suppose that g_0 belongs to the class (2.3) with $g_0(\mathbf{0}) = 0$. Let $\widehat{\mathbf{g}}_B$ and \mathbf{g}_0 be defined as in (4.4) based on B subsamples of size r , $\mathcal{B}_{r,\delta}$ be as defined in (4.3) with sample size r and hyperparameter $\delta \in \left(\frac{c_{\text{eff}}(1-c_{\text{eff}})}{2-c_{\text{eff}}}, c_{\text{eff}}\right)$. Assume Conditions 3–6 hold. Then, for any $\nu \in (1, 1 + \frac{m_0}{2})$, there exist α_{lower} and α_{upper} such that for all $\alpha \in (\alpha_{\text{lower}}, \alpha_{\text{upper}})$ and any fixed points $\mathbf{x}_*^{(1)}, \dots, \mathbf{x}_*^{(p)} \in \mathcal{B}_{r,\delta}$,

$$\sqrt{\frac{n}{r^2}} \Psi_r^{-1/2} (\widehat{\mathbf{g}}_B - \mathbf{g}_0) \xrightarrow{d} \mathcal{N}_p(\mathbf{0}, \mathbf{I}_p), \quad (4.5)$$

where α_{lower} and α_{upper} are the same as defined in Theorem 3.

For pairwise contrasts, consider the special case $p = 2$ evaluated at $\mathbf{x}_*^{(1)}$ and $\mathbf{x}_*^{(2)}$. Taking $v = (1, -1)^\top$, the corresponding pairwise variance is

$$\begin{aligned} \sigma_r^2(\mathbf{x}_*^{(1)}, \mathbf{x}_*^{(2)}) &:= v^\top \Psi_r v \\ &= \zeta_r^{(1)}(\mathbf{x}_*^{(1)}) + \zeta_r^{(1)}(\mathbf{x}_*^{(2)}) - 2\zeta_r^{(1)}(\mathbf{x}_*^{(1)}, \mathbf{x}_*^{(2)}). \end{aligned}$$

Because Condition 6 for $p = 2$ ensures the 2×2 covariance matrix is uniformly well-conditioned, the contrast variance is non-degenerate. We define the corresponding scalar normalizing factor as

$$b_{n,r}(\mathbf{x}_*^{(1)}, \mathbf{x}_*^{(2)}) := \sqrt{\frac{n}{r^2 \sigma_r^2(\mathbf{x}_*^{(1)}, \mathbf{x}_*^{(2)})}}.$$

Corollary 2. Under the conditions of Theorem 4 with $p = 2$, for any fixed pair of covariate points $\mathbf{x}_*^{(1)}, \mathbf{x}_*^{(2)}$ and any subsample scaling exponent satisfying $\alpha_{\text{lower}} < \alpha < \alpha_{\text{upper}}$,

$$b_{n,r}(\mathbf{x}_*^{(1)}, \mathbf{x}_*^{(2)}) \left\{ \widehat{\psi}_B(\mathbf{x}_*^{(1)}, \mathbf{x}_*^{(2)}) - \psi(\mathbf{x}_*^{(1)}, \mathbf{x}_*^{(2)}) \right\} \xrightarrow{d} \mathcal{N}(0, 1).$$

Since analytical forms for $\zeta_r^{(1)}(\mathbf{x}_*)$ and $\zeta_r^{(1)}(\mathbf{x}_*^{(1)}, \mathbf{x}_*^{(2)})$ are unavailable, the next theorem provides their consistent estimators.

Theorem 5. Let $\mathcal{B}_{r,\delta}$ be as defined in (4.3) with sample size r . For any two fixed evaluation points $\mathbf{x}_*^{(1)}, \mathbf{x}_*^{(2)} \in \mathcal{B}_{r,\delta}$, the following results hold.

(i) Under Condition 5, let $\widehat{\sigma}^2(\mathbf{x}_*^{(k)})$ denote the IJ variance estimator for the individual ensemble estimator $\widehat{g}_B(\mathbf{x}_*^{(k)})$, as defined in (3.8). Then, for any subsample scaling exponent satisfying $1/2 < \alpha < \alpha_{\text{upper}}$, and for $k = 1, 2$ it holds

$$\frac{n \widehat{\sigma}^2(\mathbf{x}_*^{(k)})}{r^2 \zeta_r^{(1)}(\mathbf{x}_*^{(k)})} \xrightarrow{p} 1. \quad (4.6)$$

(ii) Suppose, in addition, that Condition 6 holds. Let $\widehat{\sigma}_{1,2}^2$ denote the IJ variance estimator for the contrast $\widehat{g}_B(\mathbf{x}_*^{(1)}) - \widehat{g}_B(\mathbf{x}_*^{(2)})$, as defined in (3.9). Then, for any subsample scaling exponent satisfying $1/2 < \alpha < \alpha_{\text{upper}}$,

$$\frac{n \widehat{\sigma}_{1,2}^2}{r^2 \sigma_r^2(\mathbf{x}_*^{(1)}, \mathbf{x}_*^{(2)})} \xrightarrow{p} 1. \quad (4.7)$$

Theorem 5 shows that when $B \gtrsim n$ and $1/2 < \alpha < \alpha_{\text{upper}}$, the IJ estimator consistently estimates the covariance of the first-order Hájek projection after correcting for Monte Carlo variability from subsampling.

5 Simulation Studies

Simulation studies assess the finite-sample performance of the proposed ESM estimator for the nonparametric risk function $g_0(\mathbf{x}_*)$ and the log-hazard ratio $g_0(\mathbf{x}_*^{(1)}) - g_0(\mathbf{x}_*^{(2)})$. For each training dataset of size n , covariates \mathbf{X}_i are generated i.i.d. from $N(\mathbf{0}, I_{10})$ and truncated componentwise to $[-3, 3]$, for $i = 1, \dots, n$. The function $g_0(\cdot)$ depends on the first three components of \mathbf{X}_i , with the remaining seven serving as noise variables. Conditional on \mathbf{X}_i , event times $T_{i,U}$ are generated from the Cox model:

$$\lambda(t \mid \mathbf{X}_i) = 0.1 t \exp\{g_0(\mathbf{X}_i)\},$$

while censoring times $T_{i,C}$ are generated independently from an exponential distribution with the rate chosen to yield approximately 30% censoring. For various levels of functional complexity, we consider three forms of g_0 .

Case 1 (Linear).

$$g_{0,1}(\mathbf{x}) = x_1 - 1.2 x_2 + 0.8 x_3.$$

Case 2 (Smooth additive nonlinear).

$$g_{0,2}(\mathbf{x}) = 0.7 x_1 - 0.5 x_3 + 0.4 x_2^2 + 0.3 x_1 x_2.$$

Case 3 (Compositional nonlinear).

$$\begin{aligned} g_{0,3}(\mathbf{x}) &= 0.7 x_1 - 0.8 x_3 + 0.5 x_2^2 + \sin(0.5 x_1 x_2) \\ &\quad + 1.2 \exp\left(-0.25(x_1 - 1)^2 - 0.25(x_2 + 1)^2\right) - 1.2 \exp(-0.5). \end{aligned}$$

An independent test set $\{\mathbf{x}_{\text{test},i}\}_{i=1}^{80}$ is generated i.i.d. from $N(\mathbf{0}, I_{10})$, truncated componentwise to $[-3, 3]$, and held fixed across replications. For each training dataset, $\hat{g}_B(\mathbf{x}_{\text{test},i})$ and its bias-corrected IJ variance estimate are computed. The settings are

$$n \in \{800, 1000\}, \quad r = \lfloor n^\alpha \rfloor, \quad \alpha \in \{0.85, 0.90, 0.95\},$$

with 200 Monte Carlo replications per configuration. The log partial likelihood in (3.2) is optimized in PyTorch (Paszke et al., 2019). Each ensemble uses $B = 1000$ subsamples, and each base learner is a DNN with architecture $(p_0, 128, 64, 1)$, weight decay 0.02, learning rate 0.1, 500 epochs, and dropout 0.1, with $p_0 = 10$. For pointwise inference on $g_0(\mathbf{x}_{\text{test},i})$, performance is summarized by

Table 1: Simulation summary for pointwise inference on $g_0(\mathbf{x})$ across test points. EmpSD is the empirical standard deviation of $\hat{g}_B(\mathbf{x})$ over replications. SE is the mean estimated standard error. CP is the empirical coverage probability of nominal 95% intervals, and AIL is the mean interval length.

Case	Setting	Bias	MAE	EmpSD	SE	CP	AIL
1	$n = 800, r = \lfloor n^{0.85} \rfloor$	-0.02	0.36	0.48	0.50	0.87	1.98
	$n = 800, r = \lfloor n^{0.90} \rfloor$	-0.02	0.21	0.45	0.48	0.92	1.86
	$n = 800, r = \lfloor n^{0.95} \rfloor$	-0.03	0.11	0.40	0.44	0.95	1.72
2	$n = 800, r = \lfloor n^{0.85} \rfloor$	0.11	0.26	0.47	0.49	0.89	1.91
	$n = 800, r = \lfloor n^{0.90} \rfloor$	0.05	0.14	0.42	0.44	0.93	1.74
	$n = 800, r = \lfloor n^{0.95} \rfloor$	0.04	0.11	0.36	0.40	0.95	1.59
3	$n = 800, r = \lfloor n^{0.85} \rfloor$	0.01	0.28	0.48	0.49	0.89	1.93
	$n = 800, r = \lfloor n^{0.90} \rfloor$	0.05	0.17	0.44	0.46	0.92	1.81
	$n = 800, r = \lfloor n^{0.95} \rfloor$	0.02	0.14	0.40	0.43	0.94	1.68
1	$n = 1000, r = \lfloor n^{0.85} \rfloor$	-0.03	0.26	0.41	0.42	0.89	1.66
	$n = 1000, r = \lfloor n^{0.90} \rfloor$	-0.05	0.15	0.37	0.39	0.93	1.52
	$n = 1000, r = \lfloor n^{0.95} \rfloor$	-0.03	0.06	0.34	0.36	0.95	1.40
2	$n = 1000, r = \lfloor n^{0.85} \rfloor$	0.09	0.19	0.39	0.40	0.91	1.58
	$n = 1000, r = \lfloor n^{0.90} \rfloor$	0.04	0.10	0.35	0.36	0.94	1.41
	$n = 1000, r = \lfloor n^{0.95} \rfloor$	0.06	0.12	0.31	0.33	0.93	1.29
3	$n = 1000, r = \lfloor n^{0.85} \rfloor$	0.02	0.23	0.41	0.42	0.89	1.64
	$n = 1000, r = \lfloor n^{0.90} \rfloor$	-0.00	0.12	0.37	0.38	0.92	1.49
	$n = 1000, r = \lfloor n^{0.95} \rfloor$	0.03	0.15	0.33	0.35	0.92	1.40

bias, mean absolute error (MAE), empirical standard deviation (EmpSD), corrected IJ standard error (SE), coverage probability (CP), and corrected average interval length (AIL), averaged over the test points. For contrast inference, we consider $\psi(\mathbf{x}_{\text{test},i}, \mathbf{x}_{\text{test},j}) = g_0(\mathbf{x}_{\text{test},i}) - g_0(\mathbf{x}_{\text{test},j})$, where (i, j) index two distinct test points selected from the same test set. We focus on pairs satisfying $g_0(\mathbf{x}_{\text{test},i}), g_0(\mathbf{x}_{\text{test},j}) \in [-1.5, 2.0]$ and $|g_0(\mathbf{x}_{\text{test},i}) - g_0(\mathbf{x}_{\text{test},j})| \approx 1.0$, which represent moderate signal levels and contrasts commonly encountered in the design. We report the same metrics for $\hat{\psi}$. Figure 2 shows a representative visualization for Case 3. Table 1 summarizes pointwise inference,

and Table 2 summarizes contrast inference.

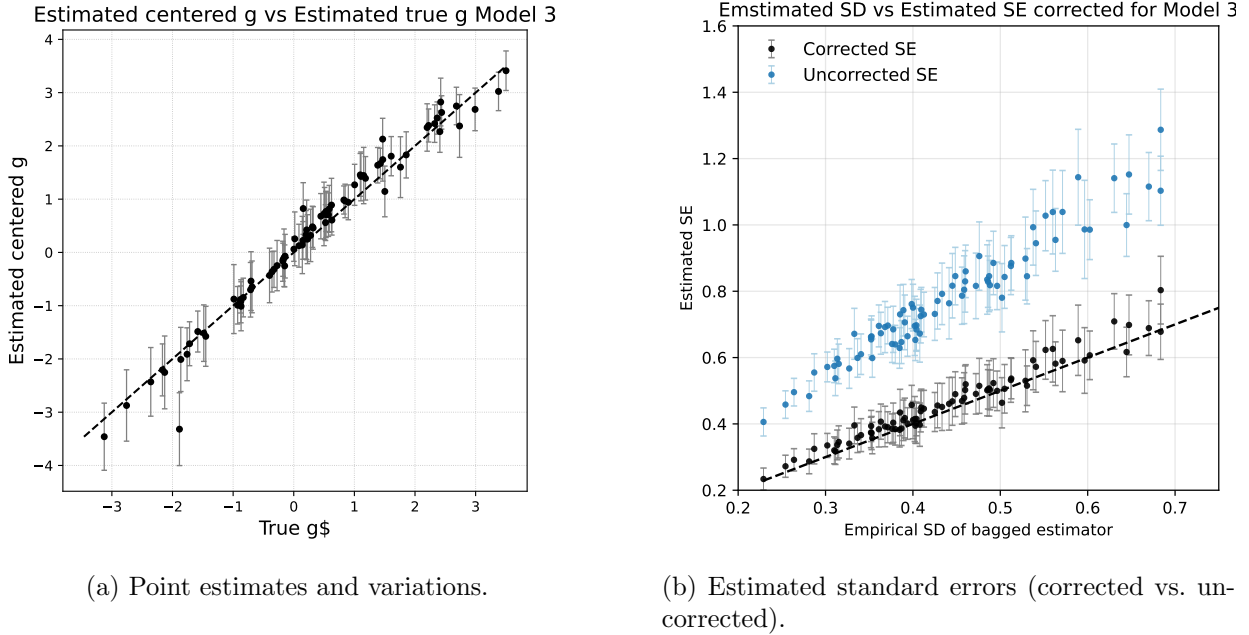


Figure 2: Estimation and inference summary for Model 3 with $n = 800$, $r = \lfloor n^{0.90} \rfloor$, $B = 1000$, DNN architecture $(p_0, 128, 64, 1)$. Panel (a) plots $\hat{g}_B(\mathbf{x})$ versus $g_0(\mathbf{x})$ across test points. Panel (b) compares EmpSD with the estimated SE, highlighting corrected and uncorrected versions when available.

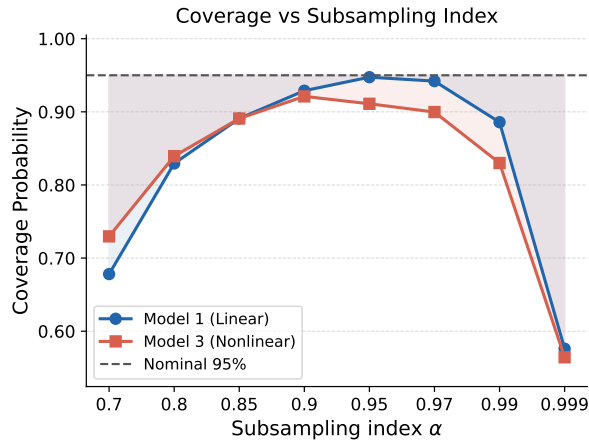
Overall, the pointwise bias is small relative to stochastic variation. For moderately large α (e.g., $\alpha \in [0.90, 0.95]$), the corrected IJ standard error closely matches the empirical standard deviation, yielding near-nominal coverage. In this regime, α is large enough to suppress approximation bias ($\alpha > \alpha_{\text{lower}}$) while remaining below the threshold required for Hájek domination and asymptotic normality ($\alpha < \alpha_{\text{upper}}$).

Figure 3 illustrates the full empirical spectrum. For smaller values ($\alpha \leq 0.8$), coverage deteriorates due to elevated approximation bias, consistent with the theoretical lower bound. In contrast, as α approaches 1, coverage collapses despite relatively stable MAE. This breakdown reflects the failure of the asymptotic Gaussian approximation as subsamples become highly overlapping. Correspondingly, the corrected standard error deviates from the empirical standard deviation in this regime, providing empirical evidence for the necessity of the upper bound α_{upper} .

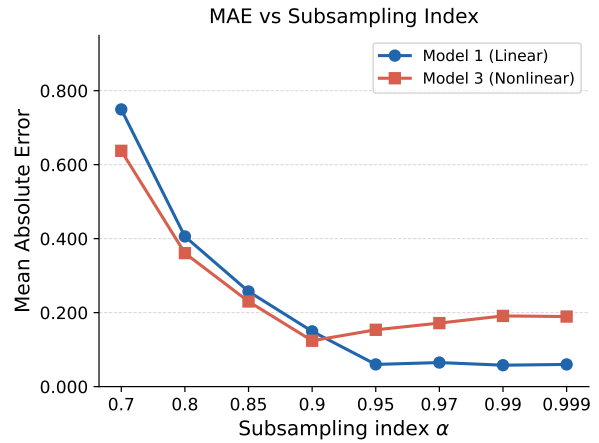
Finally, increasing the sample size from $n = 800$ to $n = 1000$ improves estimation efficiency, as reflected by reductions in the empirical standard deviation (EmpSD) and the average interval length. In addition, contrast inference achieves coverage closer to the nominal level than pointwise inference. This improvement is attributable to partial bias cancellation in the contrast, and remains evident even under the strongly nonlinear Model 3.

5.1 Comparison with Competing Methods

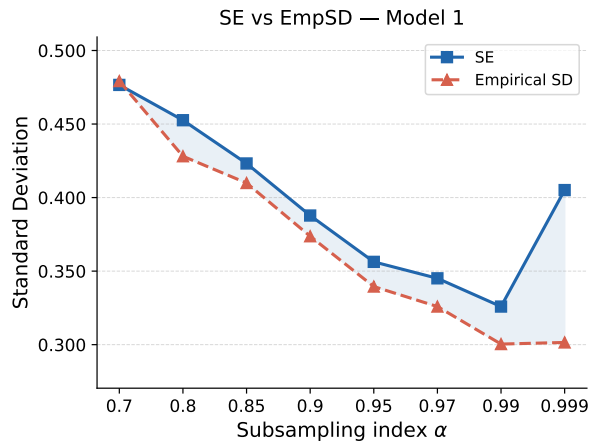
ESM (with $r = \lfloor n^{0.95} \rfloor$) is compared with the Cox proportional hazards model (CoxPH), Random Survival Forest (RSF), Gradient Boosting Regression (GBR), and DeepSurv. Table 3 summarizes



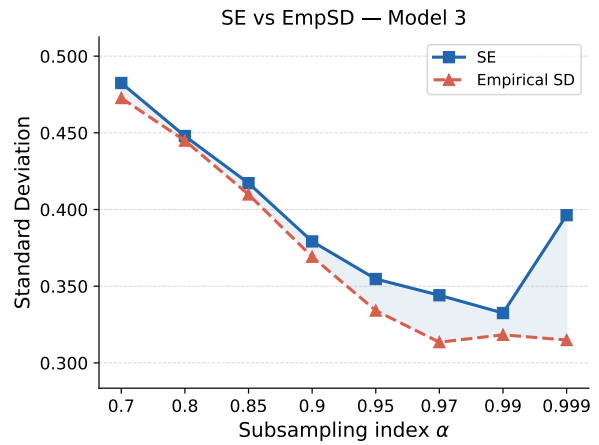
(a) Coverage Probability



(b) Mean Absolute Error



(c) SE vs EmpSD (Model 1)



(d) SE vs EmpSD (Model 3)

Figure 3: Empirical performance across the subsampling index α . At smaller values ($\alpha \leq 0.8$), high MAE degrades the CP, validating the theoretical lower bound α_{lower} . Conversely, as $\alpha \rightarrow 1$, the CP drops significantly despite stable MAE, and variance estimates diverge, empirically validating the upper bound α_{upper} .

Table 2: Simulation summary for inference on the log-hazard ratio contrast $\psi(\mathbf{x}_{\text{test},i}, \mathbf{x}_{\text{test},j})$.

Case	Setting	Bias	MAE	EmpSD	SE	CP	AIL
1	$n = 800, r = \lfloor n^{0.85} \rfloor$	-0.45	0.65	0.69	0.72	0.94	2.83
	$n = 800, r = \lfloor n^{0.90} \rfloor$	-0.23	0.52	0.62	0.67	0.95	2.61
	$n = 800, r = \lfloor n^{0.95} \rfloor$	-0.22	0.50	0.55	0.63	0.97	2.46
2	$n = 800, r = \lfloor n^{0.85} \rfloor$	-0.17	0.59	0.71	0.69	0.94	2.72
	$n = 800, r = \lfloor n^{0.90} \rfloor$	-0.02	0.45	0.55	0.64	0.97	2.51
	$n = 800, r = \lfloor n^{0.95} \rfloor$	0.06	0.43	0.53	0.56	0.96	2.21
3	$n = 800, r = \lfloor n^{0.85} \rfloor$	-0.22	0.41	0.47	0.49	0.92	1.92
	$n = 800, r = \lfloor n^{0.90} \rfloor$	-0.21	0.36	0.41	0.47	0.93	1.85
	$n = 800, r = \lfloor n^{0.95} \rfloor$	-0.10	0.33	0.40	0.46	0.95	1.80
1	$n = 1000, r = \lfloor n^{0.85} \rfloor$	-0.22	0.53	0.58	0.60	0.92	2.35
	$n = 1000, r = \lfloor n^{0.90} \rfloor$	-0.28	0.51	0.56	0.55	0.91	2.16
	$n = 1000, r = \lfloor n^{0.95} \rfloor$	-0.18	0.41	0.48	0.51	0.96	1.97
2	$n = 1000, r = \lfloor n^{0.85} \rfloor$	-0.06	0.41	0.50	0.57	0.97	2.24
	$n = 1000, r = \lfloor n^{0.90} \rfloor$	0.05	0.40	0.50	0.50	0.95	1.98
	$n = 1000, r = \lfloor n^{0.95} \rfloor$	0.15	0.38	0.44	0.46	0.95	1.80
3	$n = 1000, r = \lfloor n^{0.85} \rfloor$	-0.20	0.37	0.41	0.41	0.92	1.61
	$n = 1000, r = \lfloor n^{0.90} \rfloor$	-0.04	0.31	0.38	0.40	0.94	1.55
	$n = 1000, r = \lfloor n^{0.95} \rfloor$	0.02	0.28	0.35	0.38	0.96	1.48

pointwise MAE and the associated uncertainty quantification. Under the linear setting (**Case 1**), CoxPH performs well, consistent with correct model specification. ESM remains competitive, achieving coverage close to the nominal 95% level with relatively short intervals. Under the non-linear setting (**Case 3**), where the linear structure is misspecified, the advantage of ESM becomes pronounced. CoxPH maintains short intervals but exhibits reduced coverage, indicating unreliable uncertainty quantification. RSF and GBR attain lower MAE but tend to undercover, suggesting unstable variance estimation. DeepSurv achieves high coverage at the expense of wider intervals. In contrast, ESM attains lower MAE than competing methods while maintaining coverage near the nominal level with shorter intervals than DeepSurv, yielding a favorable accuracy–uncertainty tradeoff, particularly in the nonlinear setting.

6 Real Data Analysis

We analyze data from the Boston Lung Cancer Survival Cohort, restricted to patients with non-small cell lung cancer (Wang et al., 2023). The outcome is overall survival, defined as the time from diagnosis to death, with right-censoring at the last follow-up; the event indicator is recorded accordingly. Covariates include sex, age at diagnosis, smoking history (pack-years), tumor size (cm), chemotherapy status, cancer stage, and BMI. The cohort is randomly split into a 70% training set ($n = 1,454$) and a 30% inference set ($n = 623$).

The proposed ESM is compared with the Cox proportional hazards model (CoxPH), Random Forest (RF), Gradient Boosting Regression (GBR), and a standalone DeepSurv network. The ensemble uses $B = 1000$ subsamples with subsample size $r = \lfloor n^{0.90} \rfloor$, a dropout rate of 10%, and a

Table 3: Estimation Performance and Uncertainty Quantification (Replications $R = 200$, Bootstrap = 200) for Model 1 and 3. Pointwise metrics are averaged over the test set x_{test} .

Case	n	Method	MAE	EmpSD	SE	CP	AIL
Case 1	800	CoxPH	0.11	0.03	0.14	0.95	0.57
		RSF	0.69	0.02	0.20	0.53	1.03
		GBR	0.33	0.03	0.35	0.89	1.37
		DeepSurv	0.39	0.06	2.52	0.99	2.63
		ESM	0.11	0.40	0.44	0.95	1.72
	1000	CoxPH	0.10	0.03	0.13	0.95	0.50
		RSF	0.67	0.02	0.26	0.54	1.01
		GBR	0.32	0.03	0.32	0.88	1.24
		DeepSurv	0.31	0.11	0.58	1.00	2.25
		ESM	0.06	0.34	0.36	0.95	1.40
Case 3	800	CoxPH	0.60	0.02	0.15	0.31	0.58
		RSF	0.62	0.03	0.30	0.60	1.18
		GBR	0.34	0.03	0.34	0.87	1.32
		DeepSurv	0.37	0.05	0.68	0.99	2.62
		ESM	0.14	0.40	0.43	0.94	1.68
	1000	CoxPH	0.60	0.01	0.13	0.26	0.52
		RSF	0.60	0.02	0.30	0.60	1.16
		GBR	0.32	0.03	0.30	0.86	1.20
		DeepSurv	0.30	0.04	0.57	0.99	2.24
		ESM	0.15	0.33	0.35	0.92	1.40

DNN architecture $(p_0, 128, 64, 1)$. As reported in Table 4, the ensemble achieves the highest mean C-index and AUC, while maintaining the smallest standard errors among all methods. It also yields the shortest average interval lengths (AIL) for both metrics, indicating more efficient uncertainty quantification.

Table 4: Comparative Performance of Survival Models on the BLCS Inference Set

Method	Mean C	C-index SE	C-index AIL	Mean AUC	AUC SE	AUC AIL
ESM	0.7316	0.0018	0.0074	0.7987	0.0039	0.0171
DeepSurv	0.7284	0.0019	0.0076	0.7928	0.0043	0.0186
CoxPH	0.7223	0.0020	0.0080	0.7944	0.0050	0.0214
RF	0.7221	0.0020	0.0080	0.7928	0.0058	0.0247
GBR	0.7209	0.0019	0.0076	0.7865	0.0043	0.0184

Stage-specific hazard ratios (HRs) as functions of patient characteristics are shown in Figure 5. Each curve is defined relative to a reference patient (male, received chemotherapy, age 65, BMI 26, 35 pack-years), with one covariate varied at a time and others fixed at their reference values. Evaluation is performed over 50 evenly spaced values within clinically relevant ranges: age at diagnosis (45–80 years), tumor size (2–6 cm), smoking history (0–80 pack-years), and BMI (15–45 kg/m²). The HR at each value compares the risk of death to that of the reference profile; values above 1 indicate increased risk, values below 1 indicate reduced risk, and 1 indicates no difference. Uncertainty is quantified by pointwise 95% confidence bands based on the infinitesimal jackknife (IJ) covariance estimator. Confidence bands widen near the boundaries of the covariate ranges with

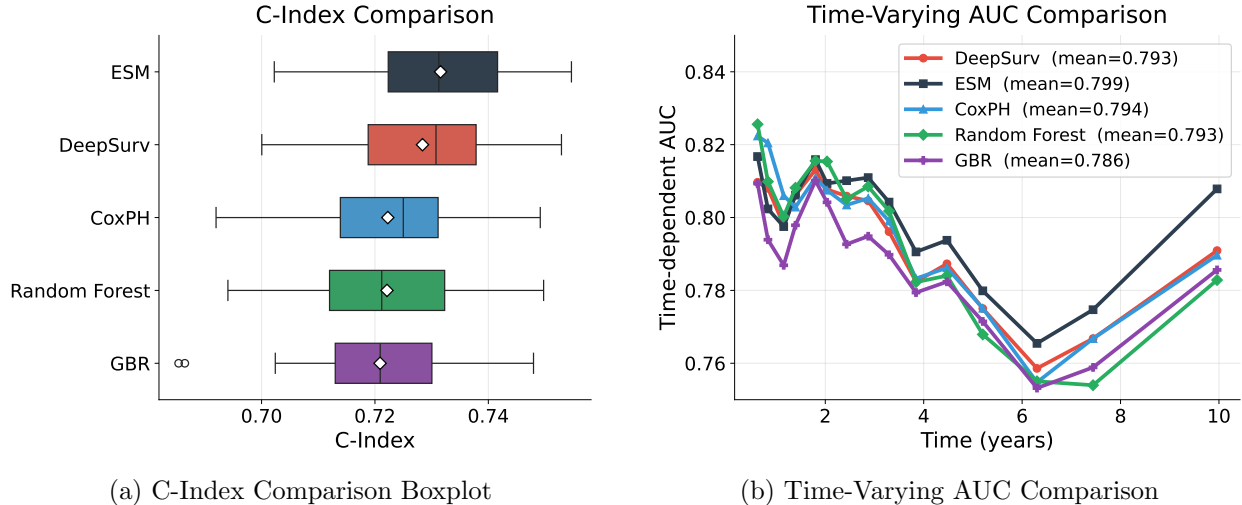


Figure 4: Comparative evaluation of model performance. The ensemble shows strong ranking stability and stable estimation accuracy over time.

reduced data support in these regions. The stage-stratified contrast analysis characterizes variation in covariate effects across stages while providing valid uncertainty quantification via the IJ-based framework.

7 Conclusion

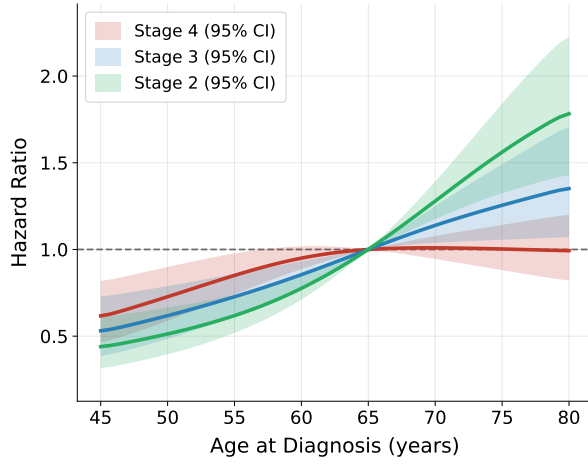
We develop a unified theoretical and inferential framework for fully nonparametric Cox models with DNNs, linking optimization-based risk bounds to ensemble-based asymptotic inference. The resulting uncertainty quantification targets contrast functionals that are often more clinically relevant than absolute risk, such as hazard ratios comparing two patients who differ in a single feature (e.g., age 70 versus 50). Our methods yield stable variance estimation and reliable finite-sample coverage, addressing limitations of standard bootstrap methods in high-dimensional settings.

Future work follows naturally from the flexibility of the ensemble framework. First, we will extend inference from the risk function $g_0(\cdot)$ to the survival function $S(t | \mathbf{x}_*)$. Since survival probabilities are nonlinear functionals of the log-hazard, the Gaussian limits for $\hat{g}(\cdot)$ enable pointwise intervals and simultaneous bands via an infinite dimensional delta method, accounting for uncertainty in both the DNN and the Breslow-type baseline hazard estimator. Second, the framework extends naturally to treatment effect estimation in time-to-event settings. Building on ensemble-based estimation ideas (Meng and Li, 2026), we define the survival Conditional Average Treatment Effect (CATE) as

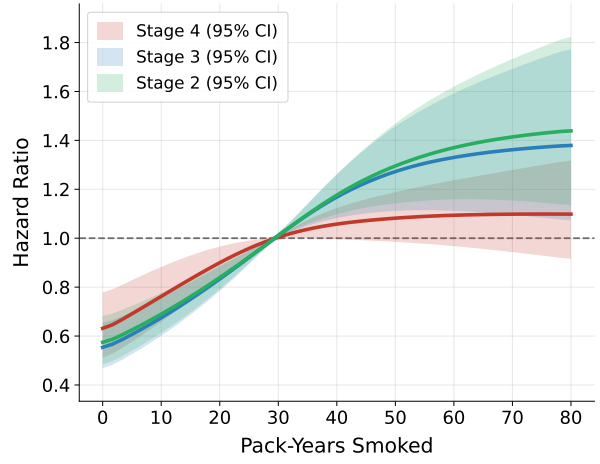
$$\tau(t | \mathbf{x}_*) = S_1(t | \mathbf{x}_*) - S_0(t | \mathbf{x}_*),$$

where $S_j(t | \mathbf{x}_*)$ denotes the conditional survival probability under treatment $j \in \{0, 1\}$. Under standard unconfoundedness conditions, this can be estimated by applying ESM separately to the treated and control cohorts. Because the groups are independent, the variance of $\hat{\tau}(t | \mathbf{x}_*)$ is the sum of the group-specific IJ variances, yielding valid Wald-type confidence intervals. A full theoretical treatment of this causal extension remains for future work.

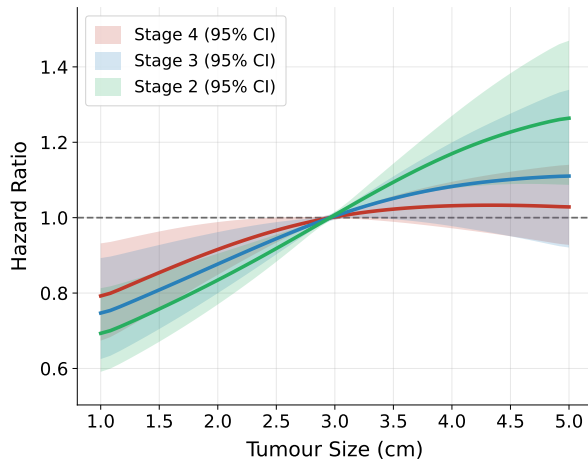
Finally, while our theory assumes controlled optimization error, further work is needed to un-



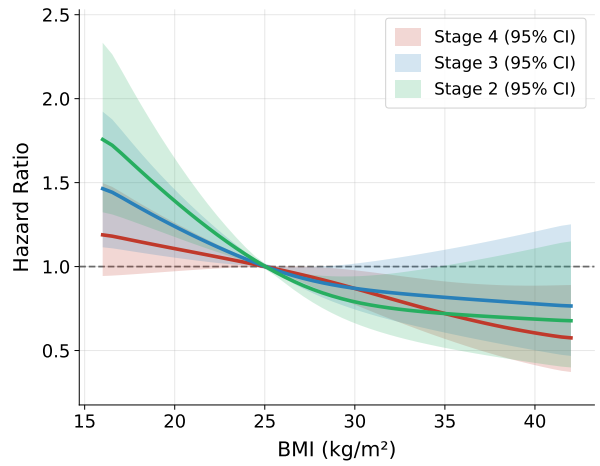
(a) Age at Diagnosis (45 to 80 years)



(b) Pack-Years (0 to 80)



(c) Tumor Size (2 to 6 cm)



(d) BMI (15 to 45 kg/m²)

Figure 5: Stage-specific contrast HR studies. In each panel, curves correspond to Stages 2, 3, and 4, with shaded regions indicating IJ-based 95% confidence bands.

derstand how implicit regularization from practical training strategies, such as early stopping and dropout, interacts with the Cox loss and affects inference.

References

- ALLEN-ZHU, Z., LI, Y. and LIANG, Y. (2019). Learning and generalization in overparameterized neural networks, going beyond two layers. In *Advances in Neural Information Processing Systems*, vol. 32.
- ANDERSEN, P. K. and GILL, R. D. (1982). Cox’s regression model for counting processes. *The Annals of Statistics* **10** 1100–1120.
- ARORA, S., DU, S. S., HU, W., LI, Z. and WANG, R. (2019). Fine-grained analysis of optimization and generalization for overparameterized two-layer neural networks. *arXiv preprint arXiv:1901.08584* .
- BICKEL, P. J., KLAASSEN, C. A. J., RITOV, Y. and WELLNER, J. A. (1993). *Efficient and Adaptive Estimation for Semiparametric Models*. Johns Hopkins University Press.
- CATTANEO, M. D., FARRELL, M. H. and FENG, Y. (2020). Large sample properties of partitioning-based series estimators. *The Annals of Statistics* **48** 1718–1741.
- CHEN, K., GUO, S., SUN, L. and WANG, J.-L. (2010). Global partial likelihood for nonparametric proportional hazards models. *Journal of the American Statistical Association* **105** 750–760.
- CHEN, S. and ZHOU, L. (2007). Local partial likelihood estimation in proportional hazards regression. *The Annals of Statistics* **35** 888–916.
- CHERNOZHUKOV, V., CHETVERIKOV, D., DEMIRER, M., DUFLO, E., HANSEN, C., NEWEY, W. and ROBINS, J. (2018). Double/debiased machine learning for treatment and structural parameters. *The Econometrics Journal* **21** C1–C68.
- COX, D. R. (1972). Regression models and life-tables. *Journal of the Royal Statistical Society: Series B (Statistical Methodology)* **34** 187–220.
- FARRELL, M. H., LIANG, T. and MISRA, S. (2021). Deep neural networks for estimation and inference. *Econometrica* **89** 181–213.
- FLEMING, T. R. and HARRINGTON, D. P. (2005). *Counting Processes and Survival Analysis*. John Wiley & Sons.
- HALL, P. (1992). *The Bootstrap and Edgeworth Expansion*. Springer Series in Statistics, Springer-Verlag.
- HOROWITZ, J. L. and MAMMEN, E. (2007). Rate-optimal estimation for a general class of nonparametric regression models with unknown link functions. *The Annals of Statistics* **35** 2589–2619.
- HUANG, J. (1999). Efficient estimation of the partly linear additive Cox model. *The Annals of Statistics* **27** 1536–1563.

- JACOT, A., GABRIEL, F. and HONGLER, C. (2018). Neural tangent kernel: Convergence and generalization in neural networks. In *Advances in neural information processing systems*, vol. 31.
- KATZMAN, J. L., SHAHAM, U., CLONINGER, A., BATES, J., JIANG, T. and KLUGER, Y. (2018). DeepSurv: Personalized treatment recommender system using a Cox proportional hazards deep neural network. *BMC Medical Research Methodology* **18** 24.
- KOHLER, M. and LANGER, S. (2021). On the rate of convergence of fully connected deep neural network regression estimates. *The Annals of Statistics* **49** 2231–2250.
- LAKSHMINARAYANAN, B., PRITZEL, A. and BLUNDELL, C. (2017). Simple and scalable predictive uncertainty estimation using deep ensembles. *Advances in Neural Information Processing Systems* **30** 6401–6413.
- MENG, X. and LI, Y. (2026). Inference for deep neural network estimators in generalized non-parametric models. *Journal of the American Statistical Association* In press.
- O’SULLIVAN, F. (1993). Nonparametric estimation in the Cox model. *The Annals of Statistics* **21** 124–145.
- PASZKE, A., GROSS, S., MASSA, F., LERER, A., BRADBURY, J., CHANAN, G., KILLEEN, T., LIN, Z., GIMELSHEIN, N., ANTIGA, L., DESMAISON, A., KÖPF, A., YANG, E., DEVITO, Z., RAISON, M., TEJANI, A., CHILAMKURTHY, S., STEINER, B., FANG, L., BAI, J. and CHINTALA, S. (2019). PyTorch: An imperative style, high-performance deep learning library. In *Advances in Neural Information Processing Systems*, vol. 32.
- SCHMIDT-HIEBER, J. (2020). Nonparametric regression using deep neural networks with ReLU activation function. *The Annals of Statistics* **48** 1875–1897.
- SLEEPER, L. A. and HARRINGTON, D. P. (1990). Regression splines in the Cox model with application to covariate effects in liver disease. *Journal of the American Statistical Association* **85** 941–949.
- STONE, C. J. (1985). Additive regression and other nonparametric models. *The Annals of Statistics* **13** 689–705.
- SUN, Y., KANG, J., HARIDAS, C., MAYNE, N., POTTER, A., YANG, C.-F., CHRISTIANI, D. C. and LI, Y. (2024). Penalized deep partially linear Cox models with application to CT scans of lung cancer patients. *Biometrics* **80** ujae022.
- VAN DER VAART, A. W. (1998). *Asymptotic Statistics*. Cambridge University Press.
- WAGER, S. and ATHEY, S. (2018). Estimation and inference of heterogeneous treatment effects using random forests. *Journal of the American Statistical Association* **113** 1228–1242.
- WANG, X., ROMERO-GUTIERREZ, C. W., KOTHARI, J., SHAFER, A., LI, Y. and CHRISTIANI, D. C. (2023). Prediagnosis smoking cessation and overall survival among patients with non-small cell lung cancer. *JAMA Network Open* **6** e2311966.
- WASSERMAN, L. (2006). *All of Nonparametric Statistics*. Springer Texts in Statistics, Springer Science & Business Media.

- WIEGREBE, S., KOPPER, P., SONABEND, R., BISCHL, B. and BENDER, A. (2024). Deep learning for survival analysis: A review. *Artificial Intelligence Review* **57** 56.
- WU, Q., TONG, X. and ZHAO, X. (2024). Deep partially linear Cox model for current status data. *Biometrics* **80** ujae032.
- YAROTSKY, D. (2017). Error bounds for approximations with deep ReLU networks. *Neural Networks* **94** 103–114.
- ZHONG, Q., MUELLER, J. and WANG, J.-L. (2022). Deep learning for the partially linear Cox model. *The Annals of Statistics* **50** 1348–1376.
- ZHOU, J., ZHANG, Y. and YU, Z. (2023). Partial linear Cox model with deep ReLU networks for interval-censored failure time data. *arXiv preprint arXiv:2307.00195* .